122 PRESSURE TRANSIENTS RESULTING FROM SODIUM-WATER REACTION FOLLOWING A LARGE LEAK IN LMFBR STEAM GENERATOR

A.K. RAJPUT
Reactor Research Centre,
Kalpakkam
India

1.0 INTRODUCTION

Tube defects in Liquid Metal Fast Breeder Reactors(LMFBR) steam generator produces sodium water reaction. Defects of steam generator heat transfer tube containing high pressure steam or water can range from a pin hole crack to a full bore rupture. The major causes[1] of such defects have been singled out as flow induced vibrations and poor quality of welds.

In most cases an efficient leak detection system, monitoring the products of reaction in secondary circuit, can give an early warning of the leakage of water from a pin hole crack, before it itself develops into a full bore opening or causes adjacent tubes to develop similar rupture as a result of wastage phenomenon. However, a design basis accident is postulated as an instantaneous full bore rupture(guillotine failoure) of a number of tubes or a single tube. The criterion for multiple tube failure relies on the phenomenon of adjacent tube wastage. Based on the experiments on sodium water reaction at different test facilities, Robin et.al.[2] concluded that adjacent tube wastage can be kept to a minimum if pitch is approximately twice the tube outside diameter. Hence, failure of a single tube has been taken as the design basis accident.

The study of sodium water reaction, following a large leak, concerns primarily with the estimation of pressure/flow transients that are developed in the steam generator and the associated secondary circuit. This paper describes the mathematical formulations used in SWRT(Sodium Water Reaction Transients) code developed to estimate such pressure transients for FBTR plant. The results, obtained using SWRT have been presented for a leak in economiser(20m from bottom water header) and for a leak in super heater portions. A time lag of 50 m sec was considered for rupture disc tubes to burst once the pressure experienced by it exceeds the set value.

Also described in annesure to this paper is the mathematical formulation for two phase transient flow for the better estimation of leak rate from the ruptured end of the damaged heat transfer tube. This leak model considers slip but assumes thermal equilibrium between the liquid and vapour phases.

2.0 SODIUM WATER REACTION ANALYSIS FOR FBTR[3]

Following guillotine failure of tube containing steam/water, pressures on the shell side of the steam generator(Fig.2) and associated secondary sodium circuit(Fig.3) exhibit a sudden increase. These pressure relief device, pressure and temperature of water, presence of secondary circuit components such as surge tank, pump etc., apart from the nature of chemical reaction. The task of predicting the functional relationships between these parameters produced the 'Sodium Water Reaction Transients' Computer Code 'SWRT' for the FBTR steam generator and associated secondary circuit.

2.1 Assumptions

The SWRT Code is an initial attempt to solve a complex problem. As in any computer code, idealisations have been made which depart from rigorous reality. Any departures from reality are believed conservative for the purpose of assessing the safety of steam generator shell and other crucial components. It is hoped that the analysis can be improved by reassessing some of those idealisations, such as,

1. Total guillotine failure of a single tube.
2. Chemical rate of sodium-water reaction much higher than the rate of steam/water influx, such that rate of energy influx is proportional to the later.
3. Reaction produces all oxides.

4. One dimensional, piston like, adiabatic growth of hydrogen bubble, since, shell diameter of FBTR steam generator is quite small ($\approx$ 177 mm).

5. Hydrogen in bubble behaves like that of an ideal gas.

6. One dimensional transients flow of sodium in secondary circuit and steam generator.

7. Magnitude of the pressure waves is such that no appreciable changes in the physical properties of sodium are caused. Hence, the wave propagation velocity roughly remains constant.

8. Adiabatic compression or expansion of argon cover gas in surge tank and expansion tank cum pump, because, in a short duration transients, practically no heat can be exchanged between cover gas control volume and its surroundings.

9. Pump speed remains unchanged during the study period of the transients($\sim$500 msec) because of high inertia of rotating parts.

10. Steam/water influx from both the ruptured ends of pipe.

11. Inertia controlled flow of water in water tube for leak in economiser/evaporator portion.

12. Fano flow model for steam leak for rupture in superheater portion.

2.2 Pressure Wave Propagation

Hydrogen generated as a result of sodium water reaction, fills, instantaneously and completely the cross-section of steam generator shell and starts pushing sodium upstream and downstream of the reaction site (Fig.4). Pressure waves emanating from sodium hydrogen interfaces of the bubble get transmitted throughout the secondary circuit and interact with its components like sodium headers on top/bottom of steam generator, surge tank, pump discharge point and expansion tank inlet etc. This phenomenon of pressure wave propagation is described Mathematically[4] by the simultaneous solution of one-dimensional transient equations of

mass balance:

$$\frac{\partial p}{\partial t} + v.\frac{\partial p}{\partial x} + \frac{\rho a^2}{g_c}\frac{\partial v}{\partial x} = 0 \qquad (1)$$

and momentum balance:

$$\frac{\partial v}{\partial t} + v.\frac{\partial v}{\partial x} + \frac{g}{\rho}\frac{\partial p}{\partial x} + \frac{f.v|v|}{2D_i} = 0 \qquad (2)$$

utilising the 'method of characteristics' with appropriate boundary conditions described by circuit components. The velocity of pressure wave propagation

$$a = C\Big/\sqrt{1 + \frac{K}{E}\frac{D_i}{t_n}} \qquad (3)$$

is lower than the sonic velocity 'C', because a part of its energy is expended in straining the pipe material.

2.3 Thermo-hydraulics of Reaction Site

The culprit responsible for the aforementioned pressure waves, is the growing high pressure hydrogen bubble and is analysed by a set of thermo-hydraulic relations describing its pressure, temperature and growth rate etc., together with leak rate models. Application of first Law of Thermodynamics and ideal gas equation of state to hydrogen in the bubble yields

$$\frac{dP}{dt} = \frac{1}{V}\left\{\frac{R\,T_0}{M} * RCF * \frac{dm}{dt} - (1+x)*P*\frac{dV}{dt}\right\} \qquad (4)$$

$$\frac{dT}{dt} = \frac{T_s - T}{m}\frac{dm}{dt} - x\frac{T}{V}\frac{dV}{dt} \qquad (5)$$

the relations describing its pressure and temperature behaviour at any time 't'. The rate of energy liberation in the hydrogen bubble depends on the rate of sodium water reaction which is proportional to the water leak rate. Of the total reaction generated heat, the energy that expends itself in generating pressure waves is represented by the bubble

expansion rate

$$\frac{dV}{dt} = S\left\{\frac{dL_w}{dt} + \frac{dL_g}{dt}\right\} \qquad (6)$$

dependent on sodium-hydrogen interface velocities,

$$\frac{dL_w}{dt} = -VND1 + \frac{g_c}{\rho a}(P - PND1) + \frac{f \cdot \delta t}{2 \cdot D_i} * VND1 * |VND1| \qquad (7)$$

$$\frac{dL_g}{dt} = +VMD1 + \frac{g_c}{\rho a}(P - PMD1) + \frac{f \cdot \delta t}{2 \cdot D_i} * VMD1 * |VMD1| \qquad (8)$$

which in turn are controlled by pressure differences inside and outside the bubble.

The effect ofnature of reaction on bubble pressure is through 'Reaction Controlling Factor'.

$$RCF = \frac{\left(\frac{m'}{M'}\right)}{\left(\frac{m}{M}\right)} \qquad (9)$$

which is the ratio of moles of hydrogen produced to the moles of water burnt. For reaction(in excess sodium and temperature > 320°C)

$$2.Na + H_2O \longrightarrow Na_2O + H_2\uparrow - 31.8 \text{ K.Cal/gm.mole}$$

leading to oxide formation, RCF is unity. This gives more amount of hydrogen produced and hence the higher bubble pressure than the reaction

$$Na + H_2O \longrightarrow NaOH + \tfrac{1}{2} H_2\uparrow - 35.2 \text{ K.Cal/gm. mole}$$

leading to hydroxide formation where RCF is one half. However, experiments[5] done by Green show that RCF is 0.6 i.e. more towards reaction leading to hydroxide formation.

2.4 Leak Rates

Various leak rate models exist for leak rate of water and that of steam for rupture in economiser and superheater portions respectively.

2.4.1 Leak in Economiser

2.4.1.1 Water leak model

Analytical models exist that predict the maximum two phase flow of saturated steam/water through tubes. A critical velocity exists at which the flow chokes at minimum area, or the tube exist, limiting the mass flow rate through the ruptured ends. Provided the external pressure is less than some specific limit, the mass flow rate is a function of the source pressure, length of tube, and the area of rupture. Although the maximum flow rate of water is predictable for a given set of conditions, the manner of reaching this maximum flow rate is not. Three simple models for predicting the flow rates upto critical velocity have been shown in Fig.5.

1. 'Conservative' model: An ultra conservative estimate of the quantity of water injected over the initial period would be obtained by assuming chocked flow exists instantaneously.
2. 'Suttering flow' model: When the tube fails, the water leaps to some velocity through the rupture. This velocity is maintained while an expansion wave travels along the tube, gets reflected from water header, and approximately doubles the rupture exit velocity every time the reflected wave returns to the rupture site.
3. 'Inertia Controlled' model: This model assumes the fluid to be incompressible and considers forces acting on an element of water in the tube. Water leaks from both the ruptured ends and accelrates upto critical velocity given by Zoludek's relation[6].

The velocity of sound in water is 1200 m/sec, so the transit time for the expansion wave to return to the rupture site has a minimum of 0.833 m.sec/m run of the tube. For a break at 20 m from bottom water header, the transit time would be 33.3 msec. In two phase mixtures, sonic velocity reduces to a very low value. This would give even longer transit times, and the stuttering flow model would predict very low flow rates for a long period following the rupture.

The first model, assuming chocked flow exists immediately following rupture, is ultra conservative and unrealistic in view of the expected transit times for the waves in the tube. The 'inertia controlled' flow model is a reasonable compromise between other two models and has been adopted in SWRT code. Balance of inertia forces with pressure forces, body forces, and frictional resistances,

$$\frac{dq_u}{dt} = \frac{g_c A}{L_u}\left\{(PH_u - PE_u) + \frac{g}{g_c}\cdot\rho_u\cdot\delta z_u - k_u\, q_{fu}^2\right\}$$

$$\frac{dq_d}{dt} = \frac{g_c A}{L_d}\left\{(PH_d - PE_d) - \frac{g}{g_c}\cdot\rho_d\cdot\delta z_d - k_d\, q_{fd}^2\right\}$$

describe the manner in which the water flow in upstream and downstream portions of the ruptured tube is accelerated upto chocked flow limit. Flashing of water occurs at the broken ends if bubble pressure is less than the saturated pressure of water. Zoludek's relation[6] gives the chocked flow rate through the broken ends

$$q = A * \sqrt{2\cdot g_c\cdot\rho\cdot\left\{PE - (1-c)\,p_{sat}\right\}}$$

$$c \doteq 0.284\,\frac{\sigma(T_u)}{\sigma(196)}$$

2.4.1.2 SWRT results for water leak

Results have been obtained by simultaneous solution of leak rate expressions and thermo hydraulic equations for reaction site together with equations describing pressure wave propagation in secondary circuit. Following a leak in the economiser portion, 20 m from bottom water header, water gushes out from both the ruptured ends. Shown in Fig.6 are the leak rates from upstream and downstream ends of the ruptured tube. Water flow accelerates upto a chocked flow limit in a time of about 200msec and during initial periods water flow rate is lower than this limit, because of its inertia and the frictional resistance it experiences inside the tube. The chocked flow limit of 6.42 kg/sec for water flow rate in the downstream portion of the ruptured tube is higher as compared to the corresponding limit of 1.65 kg/sec in the upstream portion. The short tube length of the downstream portion of the ruptured tube, hence, lesser amount of friction and higher water header pressure are the parameters which can be held responsible for this difference in chocked flow limits. The fast acceleration of water flow, in the relatively shorter downstream portion of the ruptured tube, can be attributed to lower inertia of water which is proportional to tube length.

One would expect the leak rate to go down as the hydrogen bubble pressure builds up with time. In this case it had no effect on the flow rates, since, the saturation pressure of 100 kgf/cm^2 corresponding to the water temperature of 310°C at the leak location was always higher than the bubble pressure and chocked flow conditions existed throughout. Ofcourse, if, water temperature is low, the corresponding saturation pressure would go below the bubble pressure and flow rate will decrease as hydrogen pressure builds up. It is at this point that one can feel as to how the water side temperature affects the leak rate and hence, bubble pressure and the pressure transients felt by secondary circuit and its components.

The pressure and temperature behaviour of hydrogen bubble is depicted in Fig.7. The bubble pressure continues to rise; till the transit time of 20 msec, for the compression wave, emanating from downstream sodium hydrogen interface to be reflected back as an expansion wave causes bubble to experience a sudden increase in its growth rate; thus arresting the rate of pressure rise. In general compression waves emanating from sodium hydrogen interfaces are reflected back from sodium headers, surge tank, expansion tank as expansion waves, which are responsible for the decay of bubble pressure at later times.

The position of sodium-hydrogen interfaces with time is shown in Fig.8. It can be observed that upstream interface finds it difficult to push the incoming sodium since its momentum has got to be destroyed first before it can be accelerated in the opposite direction. The downstream interface moves fast since the sodium it has to accelerate was already flowing in the same direction.

The pressure transients experienced by the bottom sodium header is shown in Fig.9. The pressure remains constant till the compression wave, emnating from the downstream sodium-hydrogen interface is experienced by it following which the pressure starts rising. The expansion wave which was reflected to the reaction site arrives back to the header as another compression wave which is responsible for further sudden increase in the header pressure. The pressure reaches a maximum of 51 Kgf/cm^2 when the expansion wave reflected from pump tank inlet causes it to fall rapidly to 29 Kgf/cm^2. Another compression wave reaching the bottom header from upstream sodium hydrogen interface via clean steam generator module causes its pressure to increase to 33 kgf/cm^2 when the rupture disc suddenly breaks after a time lag of 50 m.sec counted from the instant it acquired the set pressure of 20 kgf/cm^2. This causes the pressure to fall very rapidly almost to the sodium vapour pressure limit. The transients observed after the rupture disc has ruptured are resulting from the multiple reflections between circuit components and the reaction site. The delay of the order of 50 m.sec counted from the instant the rupture disc acquired its set pressure is based on the experiments conducted by Lions[7] et.al. The rupture discs do break at the set pressures during steady state experiments, but that does not guarantee that they will behave so during transients. We, therefore, plan to have test facility to study the rupture disc behaviour during short lived transient pressure pulses. Shown in Fig.10 is the pressure transient felt by top sodium header. The shape or the nature of transient pressure can be explained on the basis of interaction of pressure waves between circuit components and the reaction site. However, a maximum of 39 Kgf/cm^2 pressure is experienced by topsodium header.

Surge tank argon cover gas pressure and pressure at the bottom tube sheet of IHX has been shown in Fig.11. Argon cover gas pressure rises to 4.5 Kgf/cm^2 from its steady state value of 3.4 Kgf/cm^2. IHX bottom tube sheet pressure touches a maximum of 6.2 Kgf/cm^2 from its steady state value of 5.6 Kgf/cm^2 thanks to the rupture of rupture disc.

2.4.2 Leak in Super Heater

2.4.2.1 Steam leak model

Following a rupture in super heater portion steam flows towards both the broken ends in upstream and downstream portions of ruptured tube. Frictional adiabatic flow of steam has been assumed, since, during a period of few hundred m.sec. practically no heat gets transferred to steam flowing in the duct. Moreover, steam being lighter, the inertia effects caused by temporal acceleration are negligible in comparison to the inertia effects due to special acceleration, pressure and the frictional forces.

Above are the conditions required for a well known 'Fono Flow' in ducts[8]. Utilizing these Fano flow relations and techniques available for polynomial fitting, the steam flow rate

$$\frac{q - q_{max}}{q_{max}} = \sum_{m=1}^{4} C_m \left(\frac{\phi - \phi_{cr}}{1 - \phi_{cr}} \right)^m$$

is obtained as a function of pressure ratio, the critical pressure ratio and the maximum chocked flow, in the form of a fourth order polynomial.

2.4.2.2 SWRT results for steam leak

Steam leaks rates from upstream and downstream broken ends are shown in Fig.12. To begin with, since, the hydrogen bubble pressure is low, pressure ratios are less than the critical pressure ratio, and as a result steam issues from both the broken ends at critical velocity. This causes bubble pressure to shoot up immediately, thus reducing the steam flow rates to subcritical levels. Bubble pressure fluctuations are immediately felt up on the steam leak rates, unlike the water leak rate. If bubble pressure remains constant, steam leak rate also remain constant. Steam flow accelerates upto critical flow rates limits of 3.16 kg/sec and 5.45 kg/sec for upstream and downstream broken ends respectively, as bubble pressure falls.

The bubble pressure time history is shown in Fig.13. Bubble pressure remains constant till the compression wave emanating from upstream sodium hydrogen interface returns as expansion wave after experiencing reflection at top sodium header, following which it starts falling. Rupture of rupture disc and the presence of surge tank, and expansion tank causes the incident compression waves to be reflected back to reaction site as waves of expansion which are held responsible for further decay in bubble pressure as time lapses.

The positions of sodium hydrogen interfaces, with time is shown in Fig.14. The fast movement of upstream interface can be attributed to short sodium column between reaction site and top sodium header.

Pressure surges experienced by top sodium header has been shown in Fig.15. A maximum of 56.8 kg/cm^2 pressure is felt by top sodium header. The shape of this transient can be explained on the basis of interaction of pressure waves between reaction site and the circuit components.

Fig.16 shows pressure transient felt at bottom sodium header. Though this bottom header is located quite far away from the reaction site, the maximum pressure it experiences is more than that of top sodium header. Arrival of compression wave from downstream sodium hydrogen interface causes bottom header pressure to touch 53.2 kgf/cm^2 and remains constant for 15 msec or so when another compression wave emanating from upstream sodium hydrogen interface reaches via clean module. This causes another up surge and pressure reaches 75 kgf/cm^2. Very shortly after this expansion waves from expansion tank ans surge tank causes it to fall down and break in rupture disc further helps.

In Fig.17 one observes that argon cover gas pressure in surge tank rises to a maximum of 6.6 kgf/cm^2 from its steady state valve of 3.4 kgf/cm^2. This surge is higher than 4.52 kgf/cm^2, what was observed in water leak case. IHX bottom tube sheet pressure rises to 7.2 kgf/cm^2 from its steady state value of 5.6 kgf/cm^2. The corresponding maximum pressure in water leak caseras 6.2 kgf/cm^2. The proximity of IHX and surge tank to the reaction site and higher bubble pressure can be attributed to these higher values.

3.0 SODIUM WATER REACTION ANALYSIS FOR PFBR

One would have adopted computer code 'SWRT' developed for FBTR to PFBR, but for the steam generator design differences of the two units. While the design of FBTR steam generator is a serpentine once through unit, the proposed PFBR steam generator is a vertical straight tube unit, though once through concept has been retained. Shown in Fig.1 is the design of PFBR steam generator. The optimised size of one of the sixteen units is 82.5 MW. The other relevant parameters have been shown in Table-1. Of the parameters listed in Table-1, the ones which render the calculation methodology for pressure transients in steam generator of PFBR, different than that for FBTR, are larger shell of 750 mm diameter and the presence of cover gas. Based on sodium water reaction experiments[5] done inside small diameter vessels(~ 20cm), which chosed that hydrogen bubble immediately filled the cross-sectional area of the test section, one is justified with the assumption of one dimensional piston like growth of hydrogen bubble in the steam generator of FBTR which has a shell of only 177cm diameter. Since the PFBR steam generator unit has larger diameter cross-section, this type of piston like sodium ejection seems unrealistic; only part of the sodium flow cross-section will be filled by the hydrogen bubble. In fact over the initial period of growth, the shape of hydrogen bubble should almost be spherical. Detonation[5] of small charges inside tube bundles, produced an initial spherical pressure pattern with almost no preferred directional effect due to presence of close packed tubes. At later times, for a leak in the centre of the steam generator shell, the bubble gorws into elliptical and cylindrical patterns, since, hydrogen can only escape from the top of the vessel into argon cover gas space. Such a type of bubble growth results from a two-dimensional transient pressure field in the sodium surrounding the bubble. In this regard we have initiated studies on the application of the 'Method of characteristics[9]' to transient two dimensional fluid flow problems in order to estimate pressures experienced by stem generator shell of PFBR.

4.0 NOMENCLATURE

- a - Pressure wave propagation velocity
- A - Area of cross-section of heat transfer
- c - Sonic velocity in liquid sodium
- C_p - Specific heat of sodium
- Di - ID of pipe
- d - ID of heat transfer tube
- E - Youngs Modulus of Elasticity
- f - Friction factor
- g - Acceleration due to gravity
- gc - Gravitational constant
- J - Joule's Mechanical Conversion factor
- K - Bulk modulus of compressibility for sodium
- ku/kd - Friction factors for water flow in up/down stream portions of ruptured tube
- Lu/Ld - Lengths of up/down stream portions of ruptured tube
- lu/ld - Up/down stream positions of sodium hydrogen interfaces
- m/m' - Mass of water reacted and that of hydrogen produced
- M/M' - Molecular weights of water and that of hydrogen
- P - Bubble pressure
- PHD1/PLD1 - Sodium pressures Δx distances away from up/down stream sodium hydrogen interfaces at previous time step
- PEu/PEd - End pressures for up/down stream portions of ruptured tube
- PHu/PHd -- Up/down stream header pressures(steam/water side)
- ρ - Transient sodium pressure
- q_u/q_d - Water/steam leak rates from up/down stream portions of ruptured tube
- R - Universal gas constant
- S - Cross-sectional area of steam generator
- t - time
- t_h - Pipe thickness
- T - Bubble temperature
- To - Adiabatic reaction temperature(which when multiplied by heat capacity of hydrogen produced gives heat of reaction)
- Tw - Temperature of water at leak location
- V - Volume of bubble
- v - Transient flow velocity of sodium pipes etc.
- VHD1/VLD1 - Sodium velocity, Δx distances away from up/down stream sodium hydrogen interfaces at previous time step
- x - Distance along flow
- X - R/(JCpM)
- δZ - Elevation differences between leak location and steam/water headers
- ρ - Density of sodium, and that of steam/water in ruptured heat transfer tube
- σ - Surface tension of water

ANNEXURE

MATHEMATICAL MODEL FOR TRANSIENT TWO PHASE FLOW IN RUPTURED HEAT TRANSFER TUBE

The pressure of hydrogen bubble generated as a result of sodium-water reaction and the pressure transients experienced elsewhere in the secondary sodium circuit, depend on how precisely the steam/water leak rate from the ruptured heat transfer tube is estimated, apart from other parameters.

Described in this annexure are the mathematical formulations based on which a computer code is being developed to estimate the transient two phase flow behaviour in the ruptured heat transfer tube and to finally determine the leak rates from the broken ends.

The major assumption in the model is that of thermal equillibrium between liquid and vapour phases. The mechanical non-equillibrium in the model is considered through the use of slip-ratio of velocity of gas phase to that of liquid phase.

Mathematical Formulation

An instantaneous rupture of the heat transfer tube carrying high pressure steam/water, initiates expansion waves to travel along the length of the tube, upstream and downstream of reaction site. Liquid phase, following depressurisation caused by these expansion waves tend to flash into vapour phase. The analysis of transient two phase flow is performed by writing the basic conservation equations[6,11] for 1-D slip model as,

mass conservation:

$$\frac{\partial}{\partial t}\left\{\alpha \rho_g + (1-\alpha)\rho_L\right\} + \frac{\partial}{\partial z}\left\{\alpha \rho_g S u + (1-\alpha)\rho_L u\right\} = 0 \qquad (1)$$

momentum conservation:

$$\frac{\partial}{\partial t}\left\{\alpha \rho_g S u + (1-\alpha)\rho_L u\right\} + \frac{\partial}{\partial z}\left\{\alpha \rho_g S^2 u^2 + (1-\alpha)\rho_L u^2\right\} + g_c \frac{\partial p}{\partial z} + \sin\theta\left\{\rho_g \alpha + \rho_L (1-\alpha)\right\} = -\frac{\tau_w}{A} \qquad (2)$$

energy conservation:

$$\frac{\partial}{\partial t}\left\{\alpha \rho_g h^*_g + (1-\alpha)\rho_L h^*_L\right\} + \frac{\partial}{\partial z}\left\{\alpha \rho_g S u h^*_g + (1-\alpha)\rho_L u h^*_L\right\} - \frac{1}{J}\frac{\partial p}{\partial t} = \frac{q_w}{A} \qquad (3)$$

wherein stagnation enthalpies for liquid and gas phases, respectively, are

$$h^*_L = h_L + \frac{u^2}{2 g_c J} \qquad (4)$$

$$h^*_g = h_g + \frac{S^2 u^2}{2 g_c J} \qquad (5)$$

and slip ratio $S = u_g / u$ (6)

It is now assumed that vapour flashing rate is large enough so that liquid temperature instantaneously corresponds to the saturation temperature corresponding to the pressure at that location. Thus the thermal equllibrium between liquid and vapour phase is established and pressure alone is sufficient to define completely the thermo-dynamic state of each phase. Enthalpies and densities can, therefore, be expressed as functions of pressure alone and conservation equations(1)-(3) can be written, after rearrangement and simplification, as

mass conservation:

$$(\alpha \rho_g') \frac{\partial p}{\partial t} + o \frac{\partial u}{\partial t} + (\rho_g - \rho_L)\frac{\partial \alpha}{\partial t} + (\alpha S u \rho_g') \frac{\partial p}{\partial z} + (\alpha \rho_g S + (1-\alpha)\rho_L)\frac{\partial u}{\partial z} + (\rho_g S u - \rho_L u)\frac{\partial \alpha}{\partial z} = 0 \qquad (7)$$

momentum conservation:

$$(\alpha S u \rho_g')\frac{\partial p}{\partial t} + (\alpha \rho_g S + (1-\alpha)\rho_L)\frac{\partial u}{\partial t} + (\rho_g S u - \rho_L u)\frac{\partial \alpha}{\partial t} +$$

$$+ (g_c + \alpha S^2 u^2 \rho_g')\frac{\partial p}{\partial z} + (2\alpha \rho_g S^2 u + 2(1-\alpha)\rho_L u)\frac{\partial u}{\partial z} + (\rho_g S^2 u^2 - \rho_L u^2)\frac{\partial \alpha}{\partial z} = -\frac{\tau_w}{A} \qquad (8)$$

energy conservation:

$$\left(\alpha h_g^* \rho_g' - \frac{1}{J} + \alpha \rho_g h_g' + (1-\alpha)\rho_L h_L'\right)\frac{\partial p}{\partial t} + \left(\alpha \rho_g S^2 u + (1-\alpha)\rho_L u\right)/g_c J \frac{\partial u}{\partial t} + \left(\rho_g h_g^* - \rho_L h_L^*\right)\frac{\partial \alpha}{\partial t} +$$

$$\left(\alpha u S h_g^* \rho_g' + \alpha \rho_g u S h_g' + (1-\alpha)\rho_L u h_L'\right)\frac{\partial p}{\partial z} + \left(\alpha \rho_g S h_g^* + \frac{\alpha \rho_g u^2 S^3 + (1-\alpha)\rho_L u^2}{g_c J} + (1-\alpha)\rho_L h_L^*\right)\frac{\partial u}{\partial z} +$$

$$+ \left(\rho_g u S h_g^* - \rho_L u h_L^*\right)\frac{\partial \alpha}{\partial z} = \frac{q_w}{A} \qquad (9)$$

with the assumption that partial derivatives of slip(S) are negligible as compared to those for the unknowns(p, u, α).

Application of "Method of Characteristics" - MOC

It may be observed that the conservation equations(7)-(9) can be put concisely as

$$a_{ij}\frac{\partial u^j}{\partial t} + b_{ij}\frac{\partial u^j}{\partial z} + c_i = 0 \qquad (i,j = 1,\text{--}3) \qquad (10)$$

i-free ; j-dummy

Matrix components a_{ij} and b_{ij} are functions of a vector of unknowns

$$u^j = \begin{Bmatrix} p \\ u \\ \alpha \end{Bmatrix} \qquad (11)$$

The solution of equation system(10) is affected by MOC. Application of MOC[12] to equation system(10) results in compatibility relations,

$$(\sigma_i^k a_{ij})\,du^j + \sigma_i^k c_i \Delta t = 0 \qquad (i,j,k = 1,\text{--}3) \qquad (12)$$

k-free ; i,j- dummy

valid along characteristics directions

$$\frac{dz}{dt} = \lambda_k \qquad (13)$$

where, λ_k are the roots of the characteristics equation

$$|\lambda a_{ij} - b_{ij}| = 0 \qquad (14)$$

and σ_i^k are the eigen vectors corresponding to each of eigen root λ_k

Nature of roots λ_k determine whether or not the equation system(10) is amenable to MOC. Tantner and Weisman[13] have shown that with realistic slip ratios the characteristics roots are always real and distinct and hence equation system(10) is hyperbolic and is amenable to MOC.

Slip ratio computations are done using Hugmark's[14] co-relation

$$\alpha = 1/\left\{1 + (K/\alpha - 1)\frac{\rho_L}{\rho_g}\right\} \qquad (15)$$

relating (α) to quality(x). The flow factor K is a function[14] of

$$Z = \frac{R_o^{1/6} F_r^{1/8}}{\beta^{1/4}}$$

$$\left.\begin{aligned} K &= \text{Exp}\{-0.380263\,Y^2 + 1.67795\,Y - 2.104\} \quad Z \leq 10.0 \\ &= \text{Exp}\{0.09208\,Y - 0.468443\} \quad 10.0 < Z < 130 \end{aligned}\right\} \quad Y = \log_e(Z) \qquad (16)$$

The values of slip are then computed using the conventional relation

$$S = \frac{1-\alpha}{\alpha}\,\frac{x}{1-x}\,\frac{\rho_L}{\rho_g} \qquad (17)$$

In what follows is described the application of MOC for analysis of two phase flow in ruptured heat transfer tube of steam generator.

Shown in Fig.1 is the finite difference grid to determine the solution at prescribed points

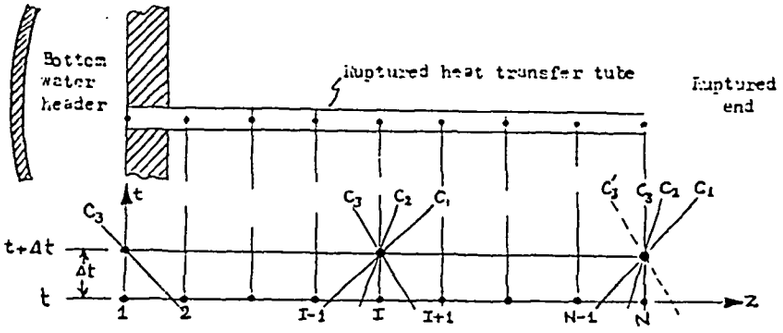

Fig.1

The mesh size ΔZ and time step Δt are related through courants[15] stability criterion i.e.

$$\Delta t \leqslant \frac{\Delta Z}{\lambda_{k\max.}} \qquad (18)$$

The compatibility relations(12) valid along characteristics lines defined by equation(13) are solved simultaneously for unknowns (p, u, α) at time ($t+\Delta t$) for an interior node I using "inverse marching method". Euler's predictor-corrector method[12] is being used to obtain converged values of these unknowns at time($t+\Delta t$).

The upstream boundary point(1), which is the bottom water header of steam generator, is described by the conditions,

$$\left.\begin{aligned} p &= p_0 \\ \alpha &= 0 \end{aligned}\right\} \qquad (19)$$

and the compatibility relation along C_3 characteristics is used to obtain the converged value of (u).

The downstream boundary point (N), which is the ruptured end, is exposed to hydrogen bubble generated as a result of sodium water reaction. Therefore, as a first step, pressure at node(N) is taken to be

$$p = p_H \qquad (20)$$

and the converged values of u and α are estimated from the simultaneous solution of compatibility relations along C_1 and C_2 characteristics. Now if the characteristics direction C_3 at node N turns out to be negative, the calculations done in the first step are correct and flow is pressure controlled, otherwise, the calculations are redone and converged values of unknowns(p, u, α) are obtained from the simultaneous solution of compatibility relations along characteristics directions C_1, C_2, C_3 and the flow is chocked at the outlet.

Based on the formulation, and methodology described in this annexure, a computer code is being developed at our end.

NOMENCLATURE FOR ANNEXURE

A	-	flow area(m^2)
De	-	internal dia of pipe(m)
$Fr = \frac{u^2}{g_c D_e} = \frac{G^2}{\rho_m^2 g_c D_e}$	-	Froude's Number
g	-	acceleration due to gravity(m/sec^2)
gc	-	gravitation conversion constant($\frac{Kg-m/sec^2}{Kgf}$)
G	-	mass flux($Kg/m^2 sec$)
h_l/h_g	-	Liquid/gas phase enthalpy(K-Cal/Kg)
J = 427	-	Joule's constant(Kgf-m/K-Cal)
p	-	pressure (Kgf/m^2)
q_w/A	-	wall heat flux(K-Cal/sec m^2)
$Re = \frac{G\ D_e}{\mu_g \alpha + \mu_l (1-\alpha)}$	-	Reynold's Number
$S \equiv \frac{u_g}{u_l} = \frac{u_g}{u}$	-	slip ratio
t	-	time(sec)
u or u_l/u_g	-	Liquid/vapour phase velocities(m/sec)
x	-	vapour quality

z - distance along fluid flow(m)

Z - A constant defined in text

$\tau_{w/A}$ - shear stress

ρ_L / ρ_g - liquid/gas phase densities(Kg/m^3)

μ_L / μ_g - liquid/gas phase viscosities (Kg/m-sec)

α - void fraction

$\beta_L = \frac{Q_L}{Q_L + Q_g} = \frac{(1-x)\rho_g}{(1-x)\rho_g + x\rho_L}$ - liquid volumetric flow fraction

Subscripts: L - Liquid phase; g - gas phase; h - homogenous; w - wall

Superscripts: $(')$ derivative w.r.to pressure

REFERENCES

1. Robin et.al. - Fast Breeder Steam Generators - S.F.E.N. Conference - Sep. 29, 1977.
2. Communication of M.G. Robin vide his letter No. DRP/EMTR/ S 69/252/GG dated August 20, 1969.
3. A.K. Rajput, "Pressure transients resulting from sodium-water reaction in steam generator of FBTR" - Design Note No. FBTR/FRG/33411/DN/20-1977.
4. Streeter, V.L., "Fluid Mechanics", McGraw Hill publication.
5. David A.Green, "Steam generator vessel pressure resulting from a sodium water reaction" - Nucl. Technology, Vol.14 June, 1972.
6. L.S. Tong, "Boiling heat transfer and two phase flow" - John Wiely and Sons - 1965.
7. Study of the sodium water reaction in the steam generator and associated circuit - M. Lions et.al. - French report No. DRP/SEMTR/CAD-R601 - Aug. 1970.
8. A.H. Shapiro, "The dynamics and thermodynamics of compressible fluid flow" - Ronald Press Company, New York, 1953.
9. Maurice, J.Z., Hoffman, J.D., "Gas Dynamics" - Vol.II, John Wiley & Sons Inc., New York - 1977 - Chapter 20 on MOC applied to steady three dimensional and unsteady two dimensional flow.
10. Hori et.al., "Sodium water reaction tests and analysis for MONJU steam generator" - Engg. of Fast Reactors for safe and reliable operation - Vol.I, Oct.1972.
11. Boure J.A., "Two phase flow and heat transfer", Hemisphere Publishing Corporation, Washington-1978(9th & 10th Chapters).
12. Maurice J.Z., Hoffman, J.D., "Gas Dynamics", John Wiley &Sons Inc. New York - 1976 - Appendix 'B' - The method of characteristics in two independent variables.
13. Tantner A, Weisman, J., "The use of method of characteristics for examination of two phase flow behaviour", Nucl. Technology Vol.38, Jan. 1978.
14. Hygmark G.A., "Hold up in Gas-liquid flow" Chem. Engg. Prog. Vol.58, No.4, 1962.
15. R. Courant and K.O. Friederichf, Supersonic Flow and shock waves Interscience Publishers, New York, 1948.

TABLE-1

	CONCEPT	CAPACTY	COVER GAS	SHELL DIA	TUBE ID/OD	No. OF TUBES	UNIT LENGTH	MATERIAL	SODIUM TEMP. (IN/OUT)	STEAM TEMP. & PRESSURE	FEED WATER TEMP.	
F.B.T.R.	ONCE THRO-UGH	12.5 (MW)	NO	177 (MM)	25.7 / 33.7 (MM)	7	90 (MT)	2¼ Cr. 1 Mo 1 Mb	510 / 280 (°C)	480 °C 125 Atm.	200 °C	
P.F.B.R.	DO	82.5 (MW)	YES	750 (MM)	10.3 / 15.8 (MM)	350	21 (MT)	2¼ Cr. 1 Mo	495 / 350 (°C)	480 °C 165 Atm.	250 °C	

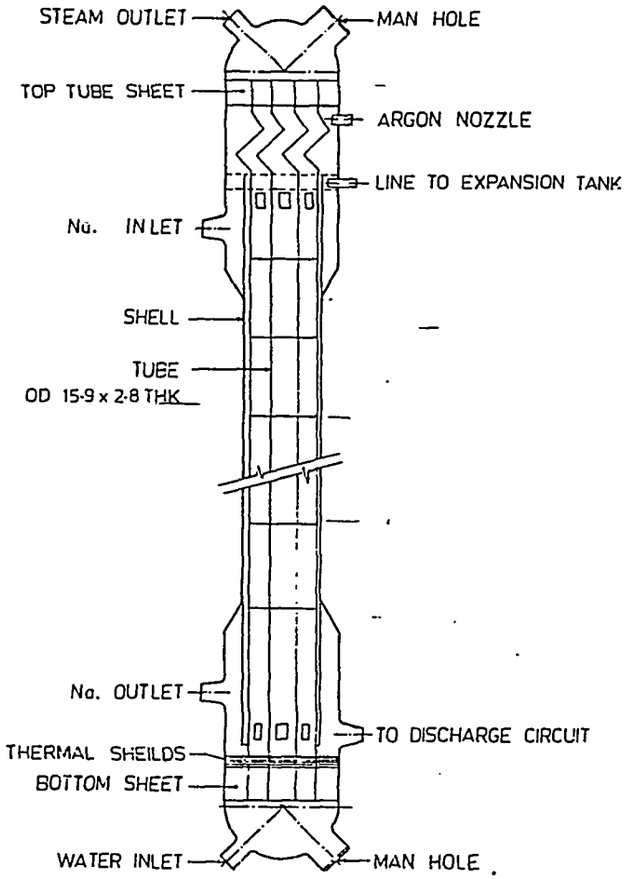

STEAM GENERATOR FOR P.F.B.R.

(RATING 82.5 MWT)

FIG : 1

F.B.T.R. STEAM GENERATOR

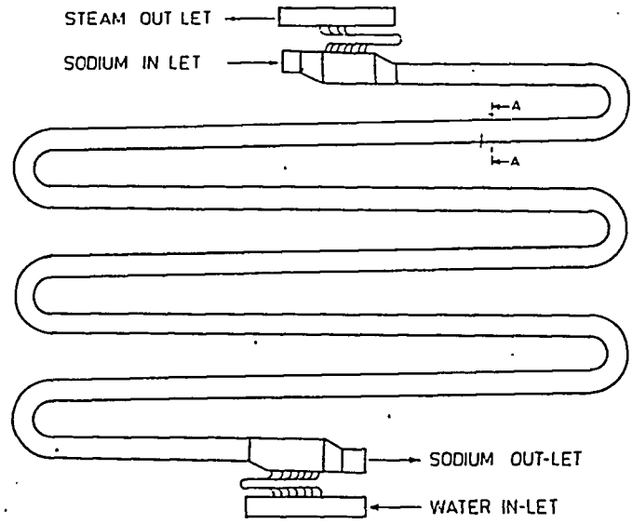

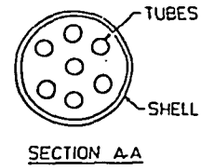

FIG. 2

F B T R SECONDARY CIRCUIT

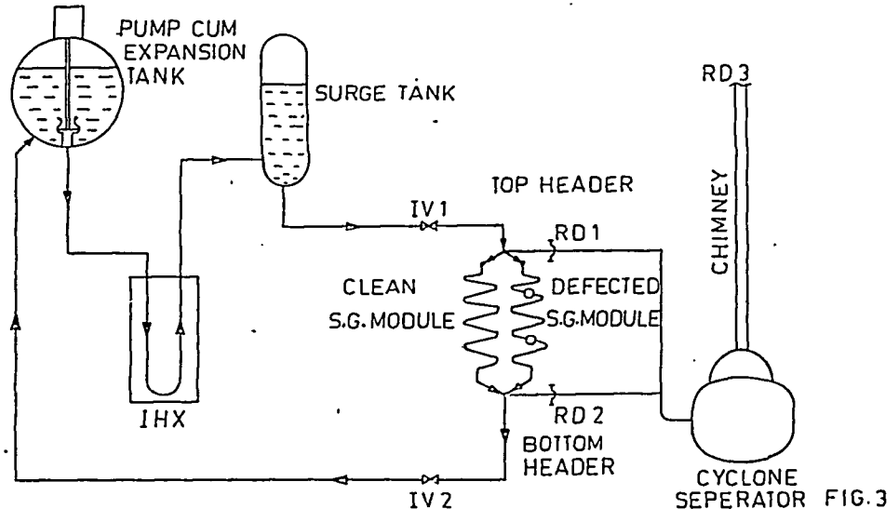

FIG. 3

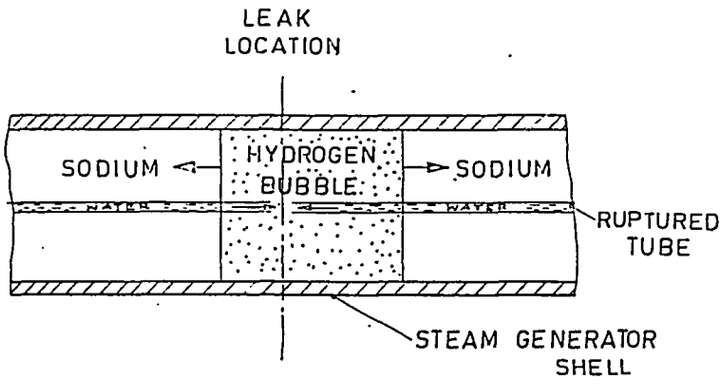
LEAK
LOCATION
SODIUM
HYDROGEN
BUBBLE
SODIUM
WATER
WATER
RUPTURED
TUBE
STEAM GENERATOR
SHELL

FIG. 4

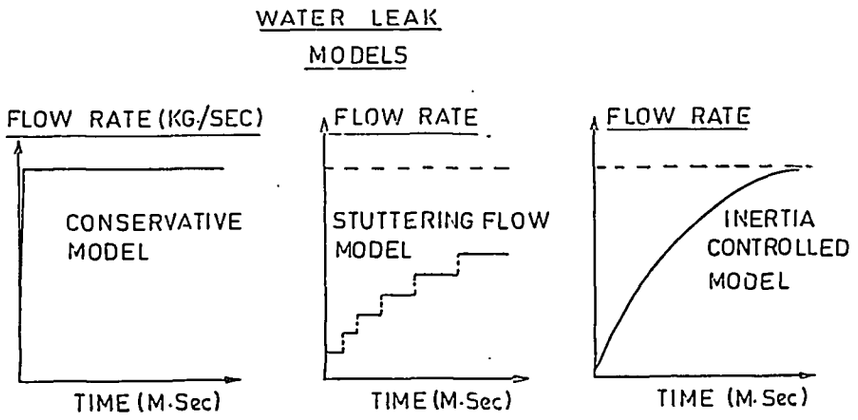
WATER LEAK
MODELS
FLOW RATE (KG/SEC)
CONSERVATIVE
MODEL
TIME (M·Sec)
FLOW RATE
STUTTERING FLOW
MODEL
TIME (M·Sec)
FLOW RATE
INERTIA
CONTROLLED
MODEL
TIME (M·Sec)

FIG. 5

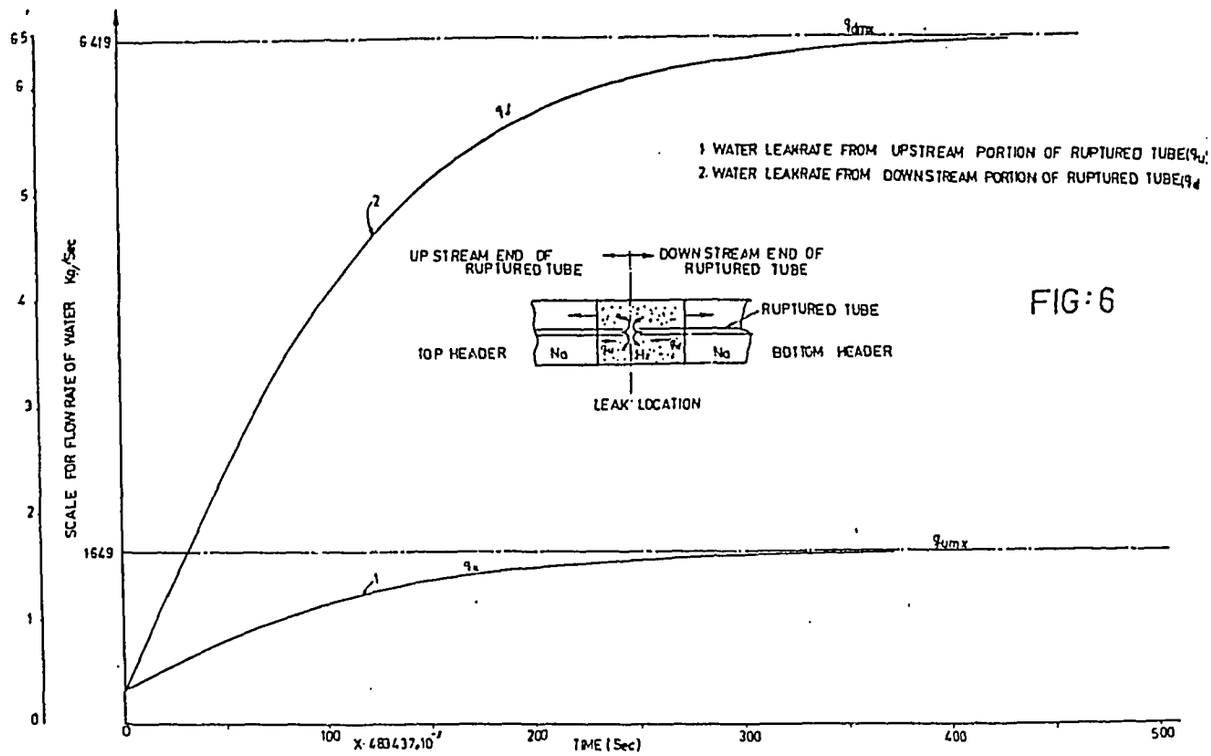
SCALE FOR FLOW RATE OF WATER Kg/Sec
6.5
6
5
4
3
2
1
0
6.419
1.649
q_{dmx}
q_{umx}
q_d
q_u
1
2
1 WATER LEAKRATE FROM UPSTREAM PORTION OF RUPTURED TUBE(q_u)
2. WATER LEAKRATE FROM DOWNSTREAM PORTION OF RUPTURED TUBE(q_d)
UP STREAM END OF RUPTURED TUBE
DOWN STREAM END OF RUPTURED TUBE
RUPTURED TUBE
TOP HEADER
Na
Hr
Na
BOTTOM HEADER
LEAK LOCATION
0
100
X·483437·10⁻²
200
TIME (Sec)
300
400
500

FIG:6

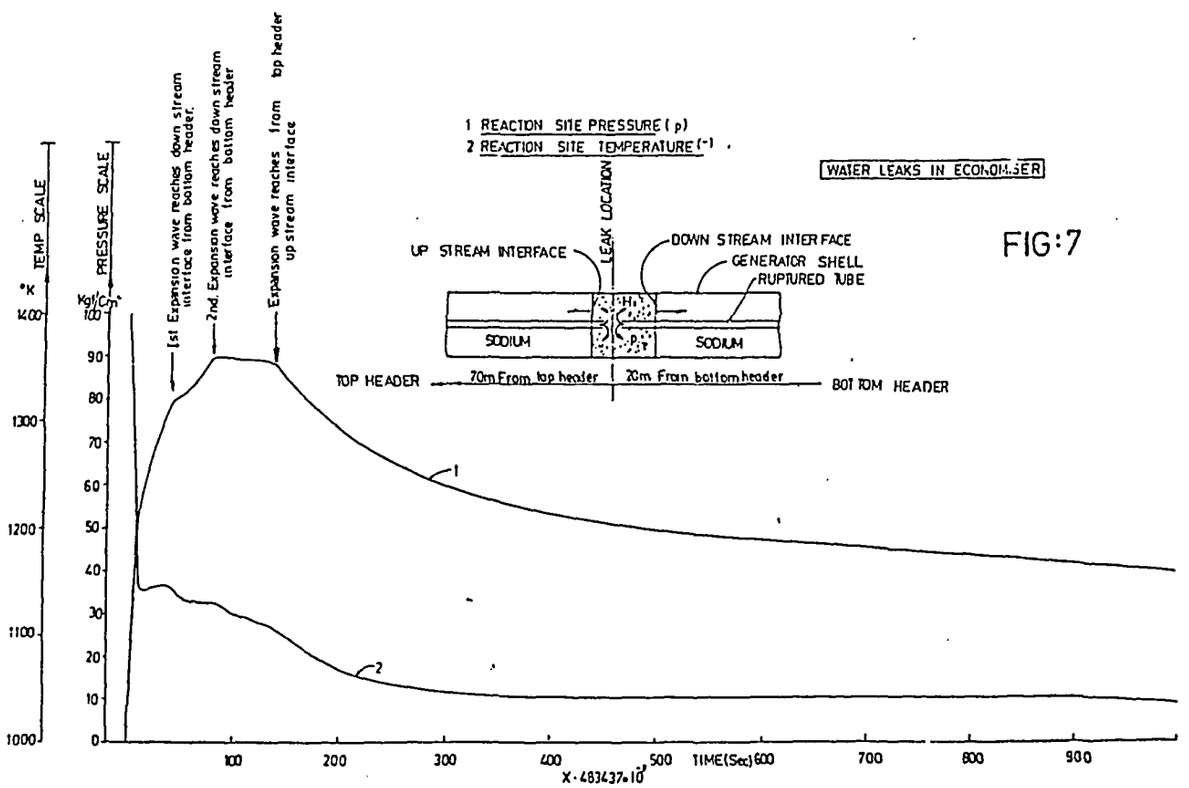
TEMP SCALE
°K
1400
1300
1200
1100
1000
PRESSURE SCALE
Kg/Cm²
100
90
80
70
60
50
40
30
20
10
0
1st Expansion wave reaches down stream interface from bottom header.
2nd. Expansion wave reaches down stream interface from bottom header
Expansion wave reaches from top header up stream interface
1 REACTION SITE PRESSURE (p)
2 REACTION SITE TEMPERATURE (T)
WATER LEAKS IN ECONOMISER
LEAK LOCATION
UP STREAM INTERFACE
DOWN STREAM INTERFACE
GENERATOR SHELL
RUPTURED TUBE
SODIUM
SODIUM
TOP HEADER
70m From top header
20m From bottom header
BOTTOM HEADER
1
2
100
200
300
400
500
TIME(Sec)
600
700
800
900
X·483437·10⁻²

FIG:7

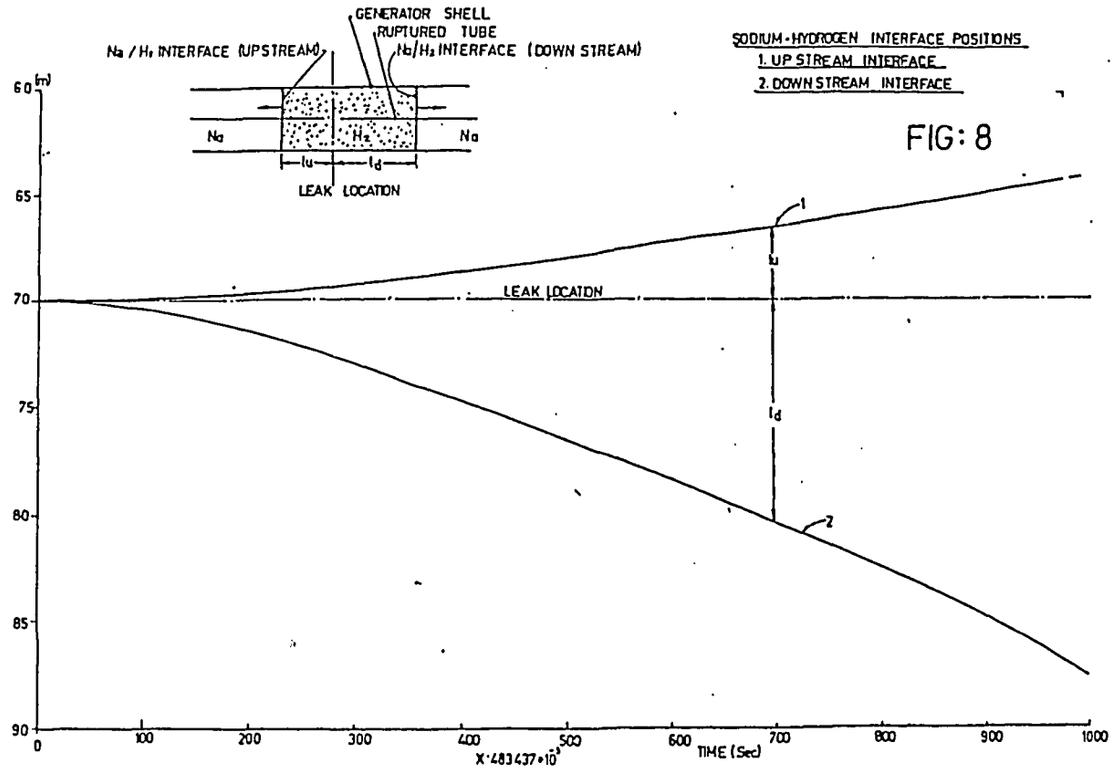
GENERATOR SHELL
RUPTURED TUBE
Na / H₂ INTERFACE (UPSTREAM)
Na/H₂ INTERFACE (DOWN STREAM)
Na
H₂
Na
lu
ld
LEAK LOCATION
SODIUM-HYDROGEN INTERFACE POSITIONS
1. UP STREAM INTERFACE
2. DOWN STREAM INTERFACE
60 (m)
65
70
75
80
85
90
1
2
LEAK LOCATION
lu
ld
0
100
200
300
400
500
600
700
800
900
1000
X·483437·10⁻⁹
TIME (Sec)

FIG: 8

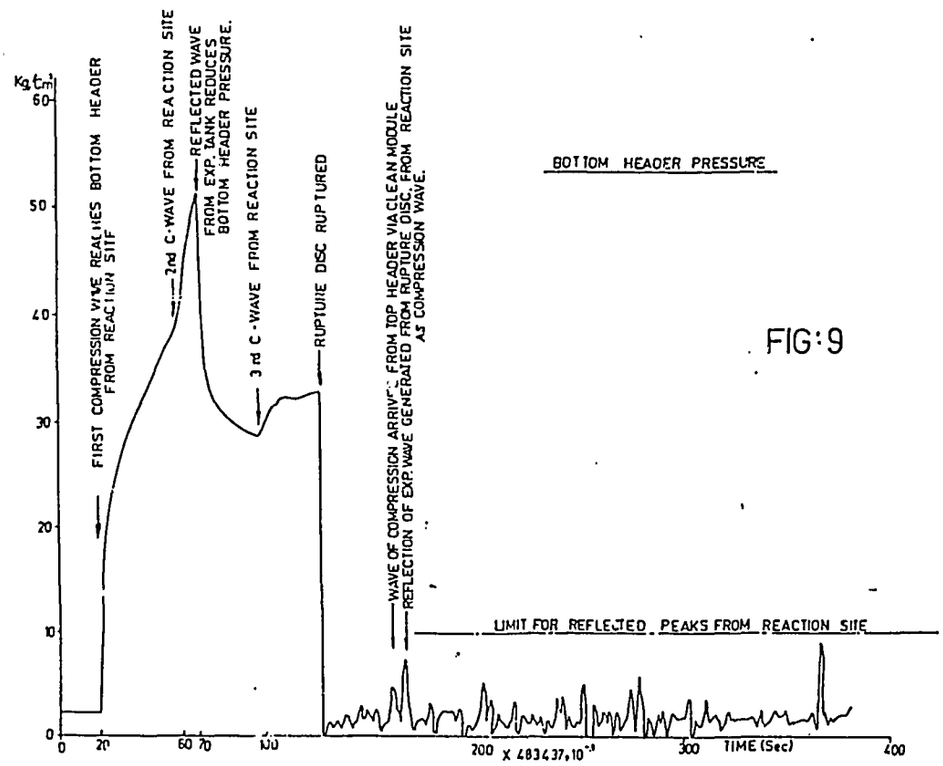
Kg/cm²
60
50
40
30
20
10
0
FIRST COMPRESSION WAVE REACHES BOTTOM HEADER FROM REACTION SITE
2nd C-WAVE FROM REACTION SITE
REFLECTED WAVE FROM EXP. TANK REDUCES BOTTOM HEADER PRESSURE.
3rd C-WAVE FROM REACTION SITE
RUPTURE DISC RUPTURED
WAVE OF COMPRESSION ARRIVES FROM TOP HEADER VIA CLEAN MODULE
REFLECTION OF EXP. WAVE GENERATED FROM RUPTURE DISC. FROM REACTION SITE AS COMPRESSION WAVE.
BOTTOM HEADER PRESSURE
LIMIT FOR REFLECTED PEAKS FROM REACTION SITE
0
20
60
70
100
200
300
400
X 483437,10⁻⁹
TIME (Sec)

FIG: 9

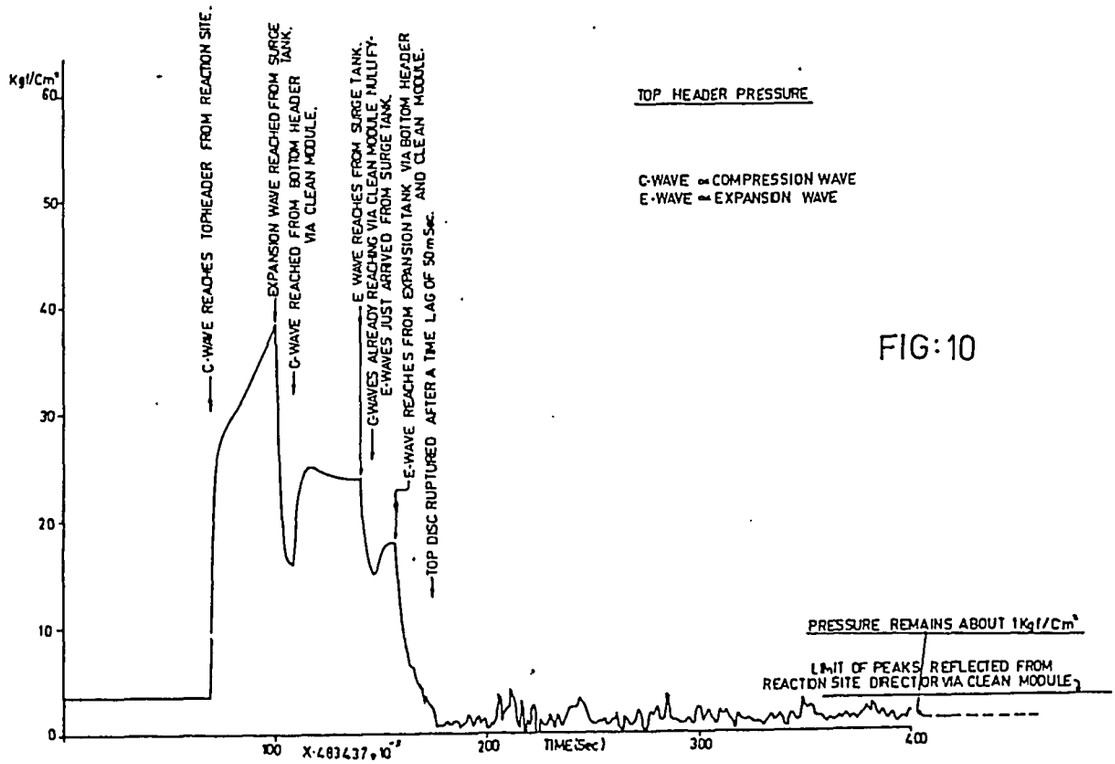
Kgf/Cm²
60
50
40
30
20
10
0
C-WAVE REACHES TOPHEADER FROM REACTION SITE.
EXPANSION WAVE REACHED FROM SURGE TANK.
C-WAVE REACHED FROM BOTTOM HEADER VIA CLEAN MODULE.
E WAVE REACHES FROM SURGE TANK.
C-WAVES ALREADY REACHING VIA CLEAN MODULE NULLIFY-E-WAVES JUST ARRIVED FROM SURGE TANK.
E-WAVE REACHES FROM EXPANSION TANK VIA BOTTOM HEADER AND CLEAN MODULE.
TOP DISC RUPTURED AFTER A TIME LAG OF 50 m Sec.
TOP HEADER PRESSURE
C-WAVE = COMPRESSION WAVE
E-WAVE = EXPANSON WAVE
PRESSURE REMAINS ABOUT 1Kgf/Cm²
LIMIT OF PEAKS REFLECTED FROM REACTION SITE DIRECTOR VIA CLEAN MODULE
100
X·483437,10⁻²
200
TIME(Sec)
300
400

FIG:10

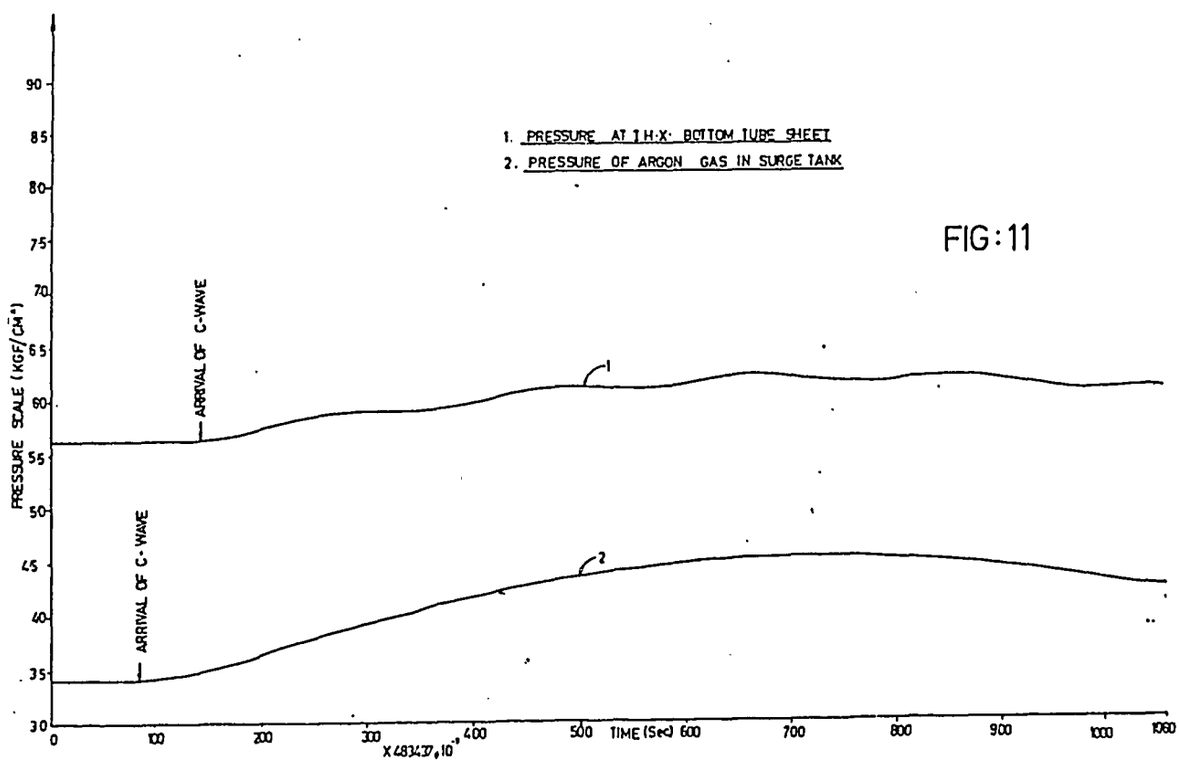
1. PRESSURE AT THX: BOTTOM TUBE SHEET
2. PRESSURE OF ARGON GAS IN SURGE TANK
PRESSURE SCALE (KGF/CM²)
90
85
80
75
70
65
60
55
50
45
40
35
30
ARRIVAL OF C-WAVE
ARRIVAL OF C-WAVE
1
2
0
100
200
300
400
500
TIME (Sec)
600
700
800
900
1000
1060
X 483437,10⁻²

FIG:11

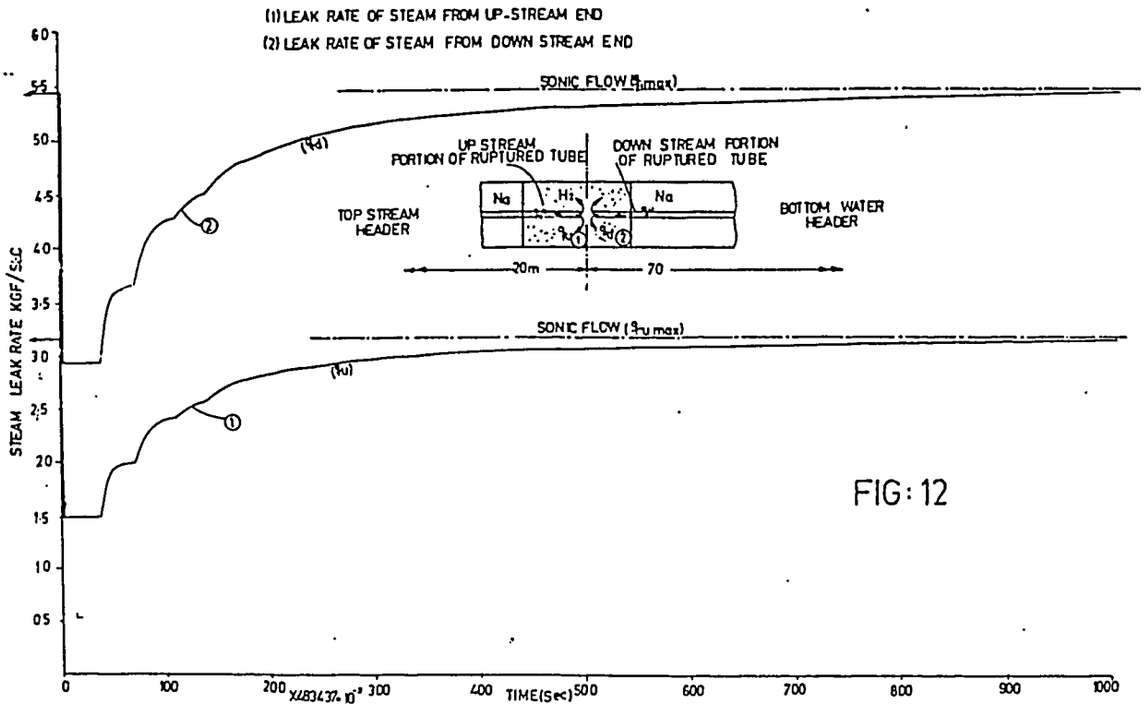
(1) LEAK RATE OF STEAM FROM UP-STREAM END
(2) LEAK RATE OF STEAM FROM DOWN STREAM END
SONIC FLOW (Gd max)
SONIC FLOW (Gu max)
UP STREAM PORTION OF RUPTURED TUBE
DOWN STREAM PORTION OF RUPTURED TUBE
TOP STREAM HEADER
BOTTOM WATER HEADER
Na
Hi
20m
70
STEAM LEAK RATE KGF/SEC
TIME (Sec)

FIG: 12

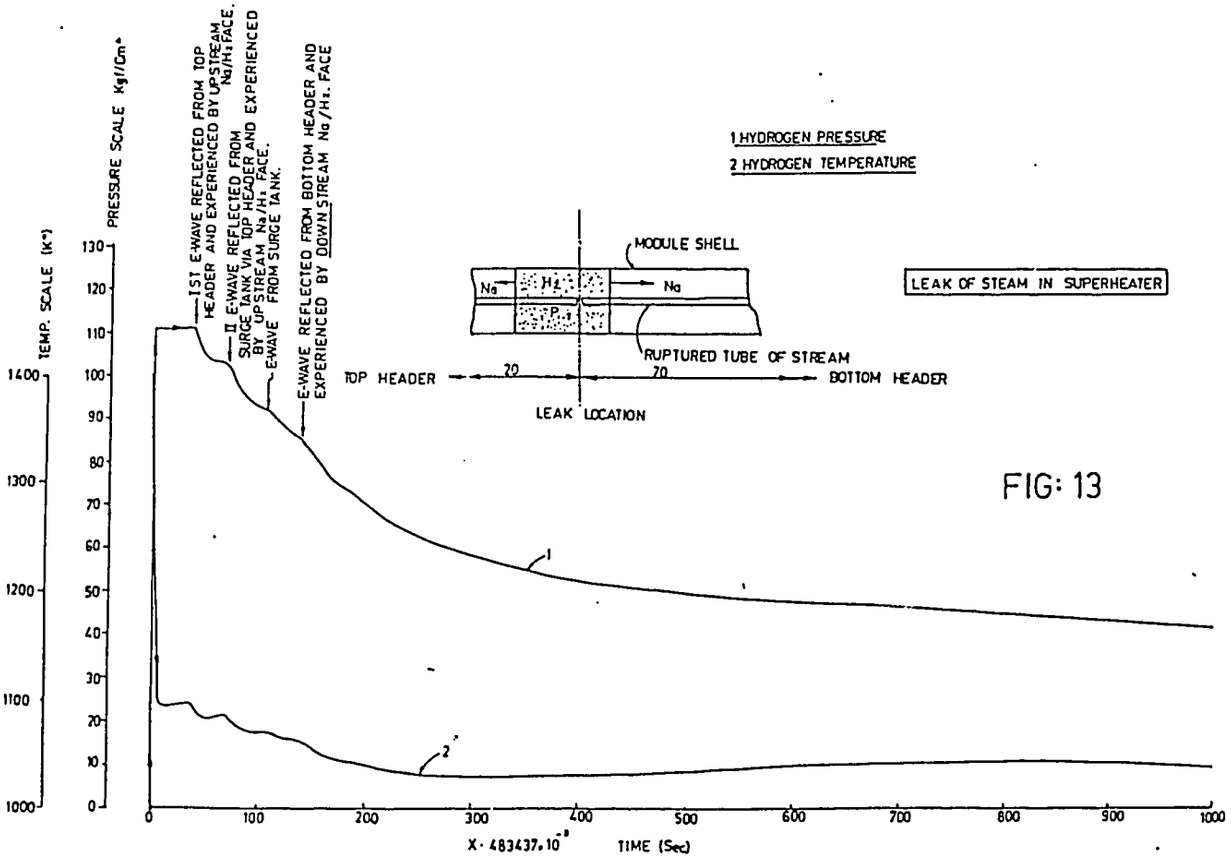
1 HYDROGEN PRESSURE
2 HYDROGEN TEMPERATURE
MODULE SHELL
LEAK OF STEAM IN SUPERHEATER
RUPTURED TUBE OF STREAM
TOP HEADER
BOTTOM HEADER
LEAK LOCATION
1ST E-WAVE REFLECTED FROM TOP HEADER AND EXPERIENCED BY UPSTREAM Na/H2 FACE.
II E-WAVE REFLECTED FROM SURGE TANK VIA TOP HEADER AND EXPERIENCED BY UPSTREAM Na/H2 FACE.
E-WAVE FROM SURGE TANK.
E-WAVE REFLECTED FROM BOTTOM HEADER AND EXPERIENCED BY DOWNSTREAM Na/H2 FACE
TEMP. SCALE (K°)
PRESSURE SCALE Kgf/Cm²
TIME (Sec)

FIG: 13

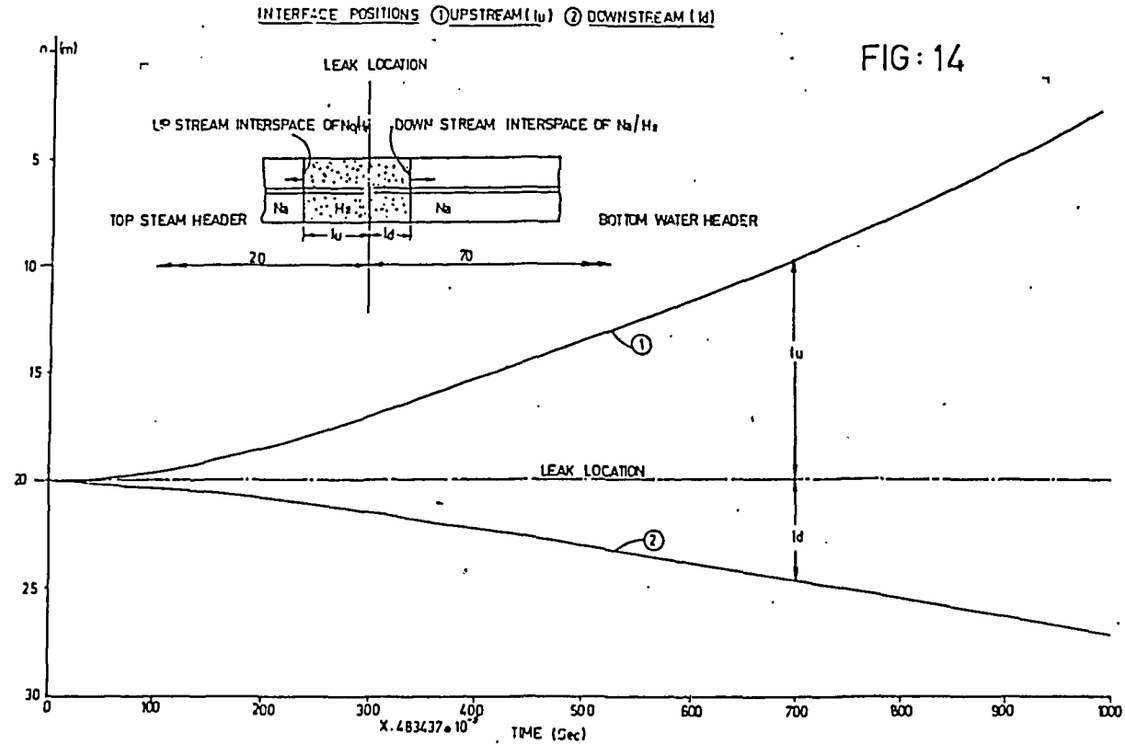
INTERFACE POSITIONS ①UPSTREAM(lu) ② DOWNSTREAM (ld)
n (m)
LEAK LOCATION
UP STREAM INTERSPACE OF Na/H
DOWN STREAM INTERSPACE OF Na/H
TOP STEAM HEADER
Na
H
Na
BOTTOM WATER HEADER
lu
ld
20
70
5
10
15
20
25
30
LEAK LOCATION
0
100
200
300
400
500
600
700
800
900
1000
X.483437.10
TIME (Sec)

FIG : 14

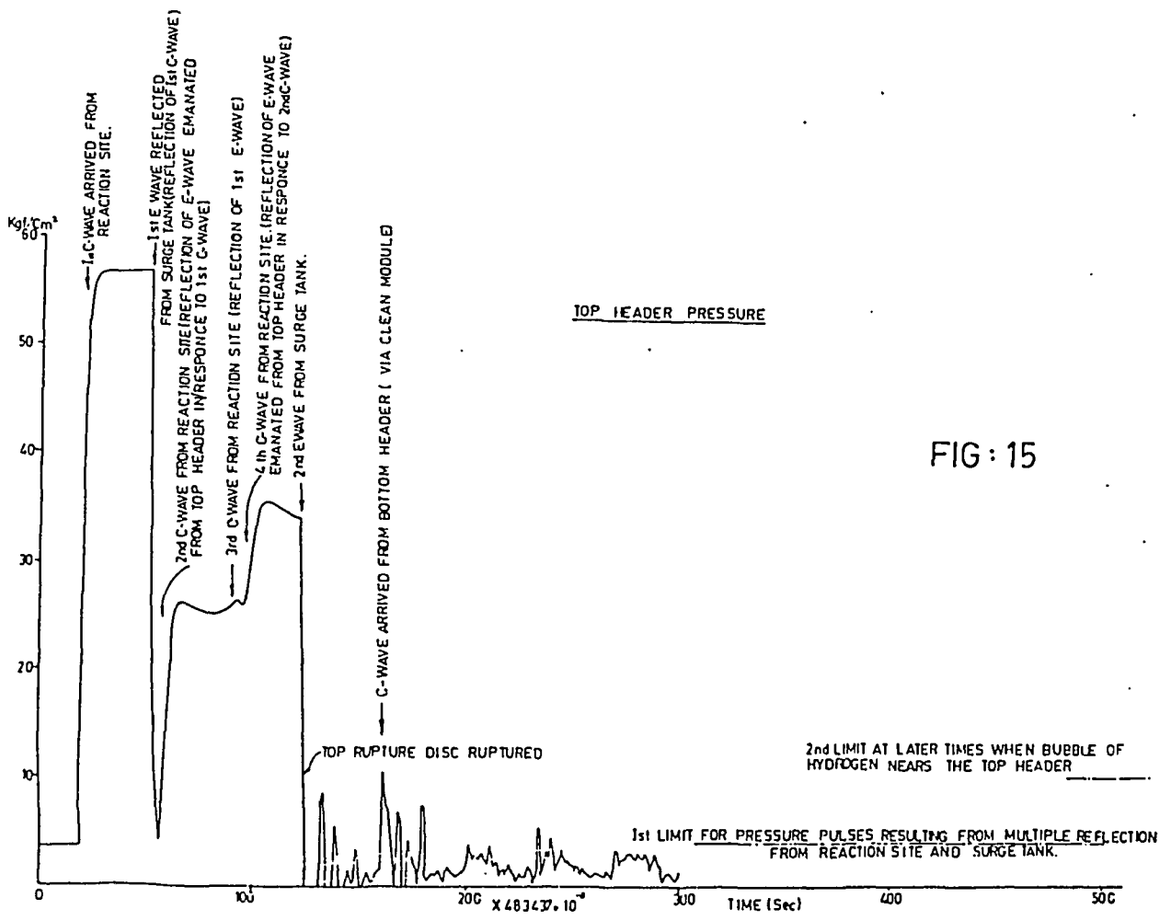
Kgf/cm²
60
50
40
30
20
10
1st C-WAVE ARRIVED FROM REACTION SITE.
1st E WAVE REFLECTED FROM SURGE TANK(REFLECTION OF 1st C-WAVE)
2nd C-WAVE FROM REACTION SITE(REFLECTION OF E-WAVE EMANATED FROM TOP HEADER IN RESPONCE TO 1st C-WAVE)
3rd C-WAVE FROM REACTION SITE (REFLECTION OF 1st E-WAVE)
4th C-WAVE FROM REACTION SITE.(REFLECTION OF E-WAVE EMANATED FROM TOP HEADER IN RESPONCE TO 2nd C-WAVE)
2nd E-WAVE FROM SURGE TANK.
C-WAVE ARRIVED FROM BOTTOM HEADER (VIA CLEAN MODULE)
TOP HEADER PRESSURE
TOP RUPTURE DISC RUPTURED
2nd LIMIT AT LATER TIMES WHEN BUBBLE OF HYDROGEN NEARS THE TOP HEADER
1st LIMIT FOR PRESSURE PULSES RESULTING FROM MULTIPLE REFLECTION FROM REACTION SITE AND SURGE TANK.
0
100
200
300
400
500
X 483437.10
TIME (Sec)

FIG : 15

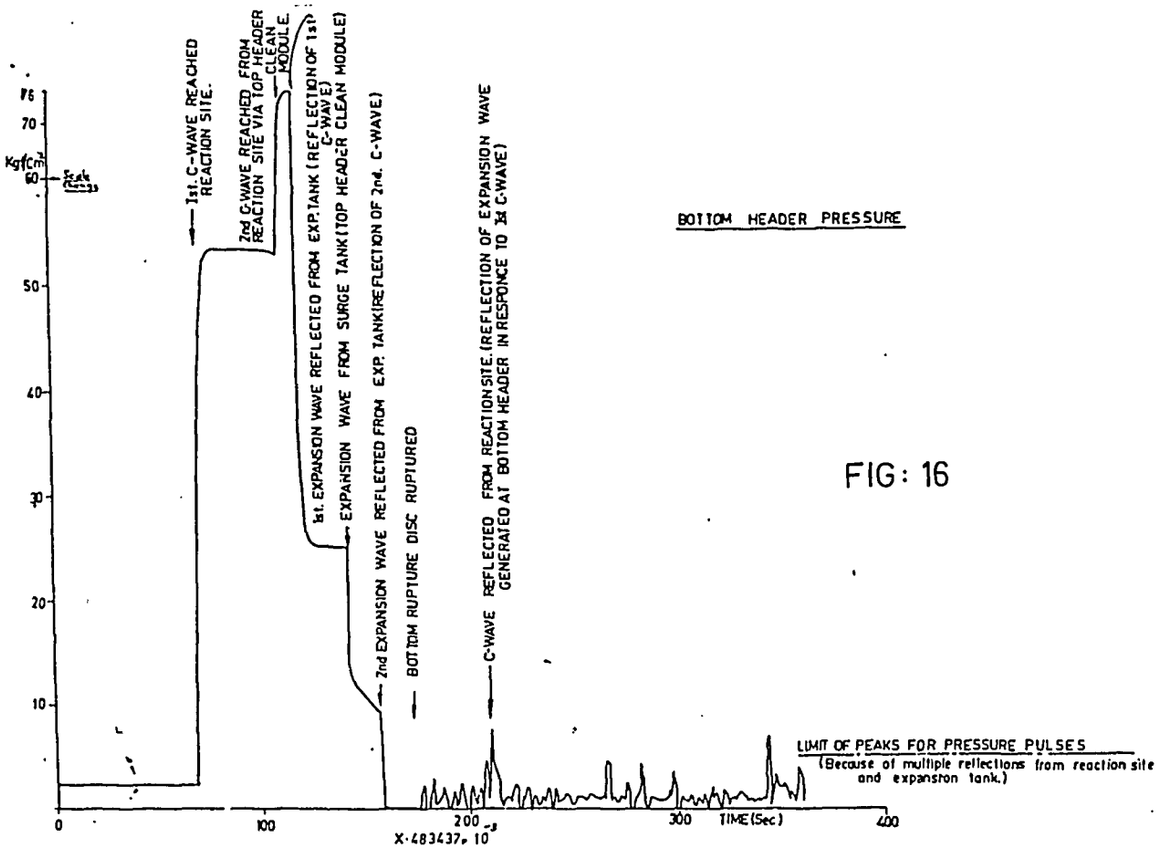
BOTTOM HEADER PRESSURE
Kgf/Cm²
70
60
50
40
30
20
10
1st. C-WAVE REACHED REACTION SITE.
2nd C-WAVE REACHED FROM REACTION SITE VIA TOP HEADER CLEAN MODULE
1st. EXPANSION WAVE REFLECTED FROM EXP. TANK (REFLECTION OF 1st C-WAVE)
EXPANSION WAVE FROM SURGE TANK (TOP HEADER CLEAN MODULE)
2nd EXPANSION WAVE REFLECTED FROM EXP. TANK (REFLECTION OF 2nd. C-WAVE)
BOTTOM RUPTURE DISC RUPTURED
C-WAVE REFLECTED FROM REACTION SITE (REFLECTION OF EXPANSION WAVE GENERATED AT BOTTOM HEADER IN RESPONCE TO 1st C-WAVE)
LIMIT OF PEAKS FOR PRESSURE PULSES
(Because of multiple reflections from reaction site and expansion tank.)
0
100
200
300
TIME (Sec)
400
X·483437, 10⁻³

FIG: 16

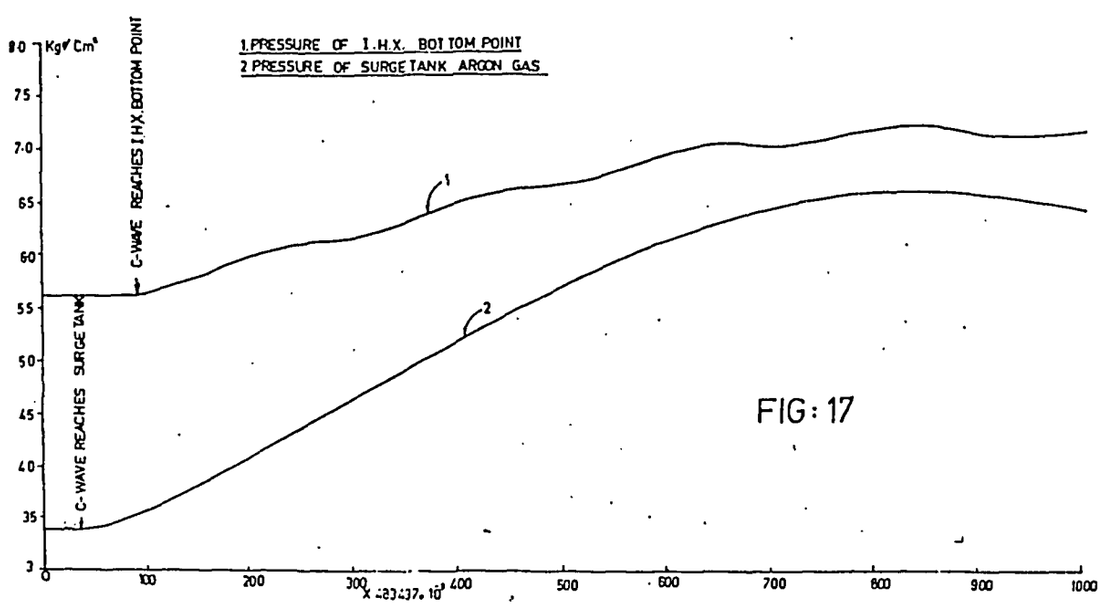
Kgf/Cm²
80
75
70
65
60
55
50
45
40
35
30
1. PRESSURE OF I.H.X. BOTTOM POINT
2. PRESSURE OF SURGE TANK ARGON GAS
C-WAVE REACHES I.H.X. BOTTOM POINT
C-WAVE REACHES SURGE TANK
1
2
0
100
200
300
400
500
600
700
800
900
1000

FIG: 17